Catalysis Science & Technology

PAPER

Cite this: *Catal. Sci. Technol.*, 2016, **6**, 6046

Self-assembled hybrid precursors towards more efficient propane ODH $NiMoO_4$ catalysts†

B. Farin,[a] P. Eloy,[b] C. Poleunis,[b] M. Devillers*[a] and E. M. Gaigneaux*[a]

Received 22nd January 2016,
Accepted 18th April 2016

DOI: 10.1039/c6cy00167j

www.rsc.org/catalysis

This work shows a novel method to synthesize bulk $NiMoO_4$ from hybrid materials made of guest ions (Ni and Mo precursors) and a polyampholytic comb-like copolymer displaying a supramolecular organization. This supramolecular organization is crucial because the copolymer serves as a nanostructuring template. While non-porous α-$NiMoO_4$ is obtained with classical methods, mesoporous β-$NiMoO_4$ is prepared here. The β-phase is more efficient in the oxidative dehydrogenation of propane (ODHP). Our strategy assumed that the properties of a catalyst strongly depend on the features of the precursor from which it comes. This is why the precursors were meticulously characterized. Homogeneous hybrids were successfully synthesized where MoO_4^{2-} anions establish electrostatic interactions with the copolymer's positive charges. The nickel cations are stabilized inside the matrix thanks to their coordination by the copolymer COO^- functions. By bridging two copolymers, such coordination bonds reinforce the copolymer organization and enable to generate the organized hybrids. Some hybrids were then calcined, characterized and tested in the ODHP reaction. Preparing the β-phase generally requires temperatures beyond 600 °C which favours sintering and makes $NiMoO_4$ poorly active. The use of supramolecularly organized precursors and the possibility it offers to form oxides under "soft conditions" lead to mesoporous β-$NiMoO_4$. The most propene selective β-$NiMoO_4$ is generated here without sacrificing its specific surface area, maintaining its remarkably high activity level. This enables reaching higher propene yields than usual.

Introduction

Answering the growing demand for sustainable and environmentally-friendly chemical processes has become a major concern. Less resource waste and more efficiency are key factors that should characterize future processes including those based on heterogeneous catalysis.[1–3] This challenge notably requires new reactor configurations but also motivates the never-ending necessity to improve the catalyst performance.[1,4,5] Therefore, various strategies can be envisaged. One widespread possibility consists of looking for new catalyst formulations.[5–8] The alternative developed here aims at the improvement of physico-chemical properties that are likely to improve the behaviour of a catalyst. More precisely, unconventional bulk NiMo-based materials are prepared and tested in the oxidative dehydrogenation of propane into propene (ODHP). This reaction has been chosen because of the interesting ability of nickel molybdates to activate propane.[9,10] Furthermore, this reaction is also in line with the efforts trying to efficiently valorise the light alkanes (C_2–C_4) coming from the huge stocks of natural gas.[11] While non-porous α-$NiMoO_4$ is produced with the usual methods, mesoporous β-$NiMoO_4$ was targeted here. This β-phase is particularly desired because of its high selectivity to propene. While quite readily obtained as a supported phase, the β-$NiMoO_4$ phase is difficult to prepare in bulk phase in a pure form.[12] Its synthesis often requires high calcination temperatures (>650 °C). This leads to poorly active catalysts due to sintering effects that diminish the specific surface area.[9,13,14] Here, the preparation of bulk β-$NiMoO_4$ is made without sacrificing the texture. Therefore, we generate NiMo-based oxides from hybrid precursors that associate inorganic ions (Ni and Mo precursors) and a polyampholytic comb-like copolymer. This matrix displays a lamellar organization thanks to hydrophobic interactions between its side chains (Scheme 1).[15,16] Taking advantage of this organization allows improving the $NiMoO_4$ textural properties. During the calcination, the matrix degradation should indeed liberate volume for pore formation.[17,18]

[a] *Institute of Condensed Matter and Nanosciences – MOlecules, Solids and ReactiviTy (IMCN/MOST), Université catholique de Louvain, Croix du Sud 2 box L7.05.17, 1348 Louvain-la-Neuve, Belgium. E-mail: michel.devillers@uclouvain.be, eric.gaigneaux@uclouvain.be*

[b] *Institute of Condensed Matter and Nanosciences – Bio- and Soft Matter (IMCN/BSMA), SUrface Characterisation Platform (SUCH), Université catholique de Louvain, Croix du Sud 1/L7.04.01, 1348, Louvain-la-Neuve, Belgium*

† Electronic supplementary information (ESI) available: This content includes a complete protocol of the XPS characterization, a detailed table (Table S1) gathering the TGA data about the hydration of the hybrids and a scheme (Scheme S1) presenting the general Ni–COO– coordination modes. See DOI: 10.1039/c6cy00167j

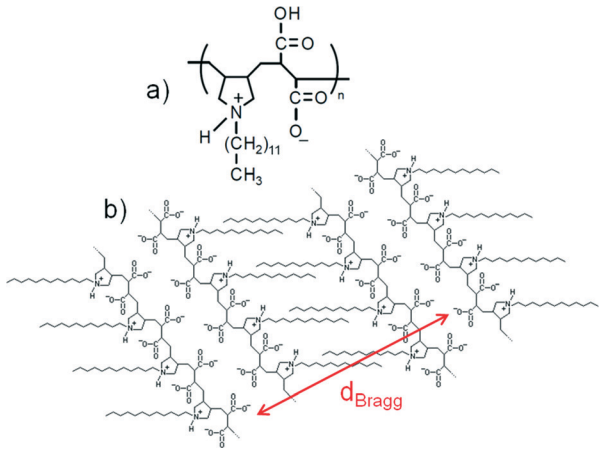

Scheme 1 (a) Model envisaged for the C12 matrix supramolecular organization. (b) Scheme redrawn from Rullens *et al.*[16]

This strategy is intended to synthesize hybrid materials without disturbing the copolymer lamellar organization. Moreover, no benefit linked to the use of a carbonaceous template can be expected without a close contact between the copolymers and the guest ions. These guest ions have to be homogeneously dispersed within the matrix. This can be warranted by ion–matrix interactions. The polyampholytic nature of the used copolymer then appears advantageous. Indeed, polyampholytes can simultaneously link cations and anions through negative and positive charges spatially separated on the same repeating unit.[19] This work is then dedicated to the preparation of homogeneous organized hybrids by taking advantage of the copolymer charges. It is aligned with preliminary investigations that were carried out by Rullens *et al.* on similar systems.[20–22] Besides, the potentiality of this original method to prepare unconventional catalysts is also evaluated here. Therefore, some hybrids are calcined and the recovered materials are characterized and tested in the ODHP reaction. The performance of these materials is finally compared to that of a reference material prepared *via* the classical co-precipitation method. Our work further illustrates the interest in using a carbonaceous template to prepare $NiMoO_4$ having properties more interesting in catalysis. In fact, our strategy assumes that the properties of a catalyst strongly depend on the features of the precursor from which it comes. As a result, having a fine knowledge about the structuration of the hybrid precursor is the key aspect of this paper.

Experimental

Preparation of materials

The used comb-like copolymer (C12 matrix) results from the alternating copolymerisation of maleic acid with a diallyl ammonium salt substituted by dodecyl side chains (Scheme 1). More details about the copolymer synthesis are available in the work of Rullens *et al.*[16] To synthesize the hybrid materials, the C12 matrix (3.36×10^{-4} mol of repeating units) was first dispersed in ethanol (10 ml). The solution was then stirred overnight before the addition of distilled water (20 ml) and the adjustment of the pH (between 6.3–6.5) by using diluted NH_3. $Ni(NO_3)_2{\cdot}6H_2O$ and $(NH_4)_6Mo_7O_{24}{\cdot}4H_2O$ were separately dissolved in distilled water (20 ml) and successively added to the copolymer solution. The pH was kept constant during the addition of the metal ions by using diluted NH_3. The final solution was stirred for 2 h and freeze-dried in order to recover the hybrid material. Various ion amounts were added to the matrix and are expressed as molar ratios of inorganic ions per copolymer repeating unit (I/R ratio) namely I/R ratio = 0, 0.25, 0.5, 1, 1.5, 2, 3 and 4. Ni and Mo were always introduced in a 1 : 1 stoichiometric ratio. Thereby, for an I/R ratio = 1, 1 mol of copolymer repeating units was mixed with 0.5 mol of nickel ions (Ni) and 0.5 mol of molybdenum ions (Mo). Hybrid precursors containing only one of the two metals were also synthesized. In such a case, an I/R ratio = 1 consisted of adding 0.5 mol of Ni or Mo ions to 1 mol of copolymer repeating units. The hybrid precursors having an I/R ratio = 1 and 4 were finally calcined for 4 h at 475 °C in air and in a muffle oven. A reference catalyst (NiMo-Cop) was also prepared *via* the co-precipitation method detailed by Del Rosso *et al.* and calcined for 4 h at 550 °C in air.[23] The reason why the NiMo-Cop catalyst was calcined at a higher calcination temperature than the catalyst obtained from the hybrid precursors is explained later.

Characterization

X-ray diffraction (XRD) was performed on a Siemens D5000 diffractometer using Cu Kα radiation (λ = 0.15418 nm). On the one hand, the C12 matrix and the hybrid materials were characterized by recording 2θ diffractograms between 0.5–10° and 10–60° at a rate of 0.12 and 0.6° min^{-1}, respectively. On the other hand, the mixed oxides were characterized by recording 2θ diffractograms between 5 and 75° at a rate of 1.2° min^{-1}. Polished Si monocrystals not diffracting in the explored angle window were used as sample holders on which the analysed powders were gently spread. The crystalline phases were identified *via* the ICDD-JCPDS database.

Fourier transform infrared spectroscopy (FTIR) was performed on an IFS55 Equinox spectrometer (Bruker) equipped with a DTGS detector and exploited in transmission mode. The spectra were recorded between 400 and 4000 cm^{-1} with a 4 cm^{-1} resolution. Transparent discs were prepared by diluting 100 times each sample with KBr (>99%, Janssens Chimica).

Thermogravimetric analyses (TGA) were performed on a Mettler Toledo TGA/SDTA 851 apparatus. The samples (about 10 mg) were heated in an air stream (30 mL min^{-1}) from 30 °C to 600 °C using a 10 °C min^{-1} rate.

X-ray photoelectron spectroscopy (XPS) was performed on a Kratos Axis Ultra spectrometer (Kratos Analytical) equipped with a monochromatized aluminum X-ray source powered at 10 mA and 15 kV. The pressure in the analysis chamber was

about 10^{-6} Pa. The analyzed area was 700 μm × 300 μm. The angle between the normal to the sample surface and the direction of the photoelectron collection was 0°. The charge stabilization was achieved by means of an electron source coaxially mounted to an electrostatic lens column. The following sequence of spectra was recorded: survey spectrum, C_{1s}, O_{1s}, N_{1s}, Ni_{2p}, Cl_{2p} and C_{1s} again. The latter was made to check the charge stability as a function of time and the absence of sample degradation during the analyses. The C-(C, H) component of the carbon C_{1s} peak was fixed at 284.8 eV to set the binding energy (BE) scale. Further details about the experimental setup can be found in the ESI.†

Static negative time-of-flight-secondary ion mass spectroscopy (ToF-SIMS) was carried out on an IONTOF V spectrometer (IONTOF GmbH, Münster, Germany). The samples were bombarded with a pulsed Bi^{3+} ion beam (30 keV). The analyzed area was a square of 500 μm^2 and the data acquisition time was 60 s. Charge effects were compensated by means of an interlaced pulsed electron flood gun (E_k = 20 eV). Thereby, the primary ion dose density was lower than 10^{11} Bi^{3+} per cm^2. The powders were supported by pressing them with a spatula onto the adhesive side of "Post-it®" pieces.

Nitrogen physisorption was performed at −196.15 °C on a Micromeritics TriStar 3000 instrument. The specific surface area of the catalysts was calculated by using the BET method between 0.05 and 0.30 $P/P°$. The BJH method was applied to extract the pore size and volume from the desorption isotherm. The samples were outgassed overnight at 150 °C under vacuum before the measurement.

Scanning electron microscopy (SEM) was performed on a LEO 983 GEMINI microscope equipped with a field emission gun. Pictures were acquired on uncoated samples with an acceleration voltage of 1 kV.

Catalytic test

The NiMo-based catalysts (0.150 g) were tested in the ODHP reaction in a U-shaped quartz reactor, at 475 °C and in a 40 mL min^{-1} total flow ($C_3H_8/O_2/N_2$ = 10/12.5/77.5 vol%). The propane stability was checked and no conversion in the presence of O_2 and without catalyst was observed. The reaction mixture was analysed using an online Varian GC. The separation, detection and quantification of the compounds (O_2, N_2, CO, CO_2, C_2H_4, C_3H_8, C_3H_6 and oxygenated products) were managed by means of 3 columns (one HayeSep column, one Molecular sieve and one EC-Waw column), one FID and one TCD. Traces of ethyl propionate, acrylic acid and acetic acid were sometimes detected but not quantified. Satisfactory carbon balances were calculated from the catalytic results. The catalytic performance is expressed in terms of propane conversion, product selectivity and propene yield. The selectivity to the products composed of less than three carbon atoms was calculated by using a stoichiometric correction coefficient (CO_2, CO, *etc.*). The product selectivities were normalized in order to get rid of the experimental variability.

Results

Characterization of hybrid materials

Each copolymer repeating unit possesses three acido-basic functions namely two COOH moieties and one tertiary amine group (Scheme 1). An acido-basic titration enabled to estimate their pK_a between 2.9–3.3, 5.5–5.9 and 8.4–8.8, respectively. These values match the data reported in the literature for similar systems.[24,25] The hybrid materials were thus prepared at pH 6.3–6.5 in order to maximize the amount of negative COO^- functions without decreasing the number of positive amine groups. Thereby, the copolymer charge number and thus its ability to link ions were both maximized.[26] Under such conditions, in the presence of ammonia, the Mo and Ni ions exist as soluble MoO_4^{2-} anions and $[Ni(H_2O)_{6-x}(NH_3)_x]^{2+}$ positive complexes, respectively.[26,27]

The diffractogram of the C12 matrix displays a low-angle Bragg peak which reveals its supramolecular organization (Fig. 1). By using Bragg's law, the position of this peak is related to an interreticular distance of 27.8 Å (d_{Bragg}) repeated along the copolymer organization (Scheme 1). The addition of Ni ions to the C12 matrix progressively shifts this peak to lower angles until reaching an I/R ratio = 1 (Fig. S1†). This shift of 2.9 Å corresponds to an increase of the C12 matrix d_{Bragg} from 27.8 Å to 30.7 Å (Fig. 2a, blue triangles) and suggests an expansion of the copolymer organization due to the insertion of Ni ions.[28] This d_{Bragg} decreases around 29.3 Å when larger nickel amounts are mixed to the matrix (I/R ratios > 1). Simultaneously, the crystallization of $Ni_2(NO_3)_2(OH)_2{\cdot}2H_2O$ and $Ni(NO_3)_2{\cdot}6H_2O$ is detected on the diffractogram of these materials (Fig. S1†). A similar increase of the copolymer d_{Bragg} is observed when Mo ions are added, in addition to the Ni ions, to the C12 matrix (Fig. 2). However, this d_{Bragg} then remains stable around 30.8 Å even if ion amounts larger than the I/R ratio = 1 are added to the matrix. In parallel, NH_4NO_3 and $(NH_4)_4[NiMo_6O_{18}(OH)_6]{\cdot}5H_2O$ start to crystallize (Fig. 1). The latter phase corresponds to a previously reported Anderson–Evans-type heteropolycompound

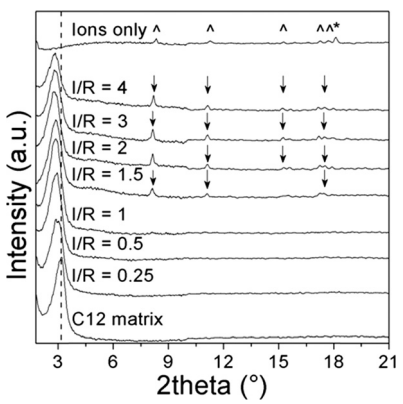

Fig. 1 Diffractograms of hybrid materials containing Ni and Mo ions. The crystalline phases identified were NH_4NO_3 (*) and $(NH_4)_4[NiMo_6O_{18}(OH)_6]{\cdot}5H_2O$ (^).

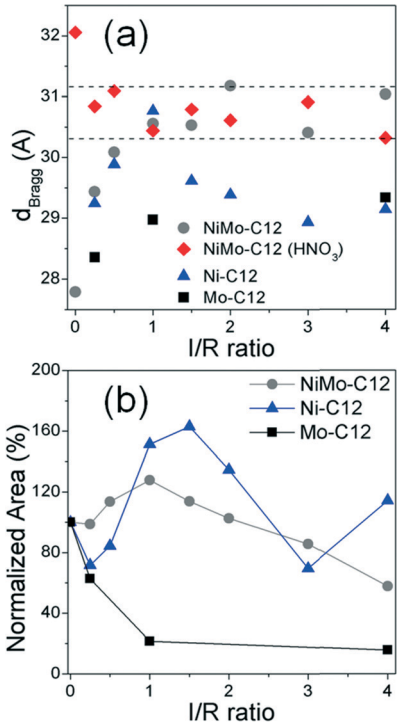

Fig. 2 Evolution of the copolymer d_{Bragg} as a function of the amount and the nature of the ions added to the C12 matrix (a). Evolution of the normalized area of the copolymer low-angle peak as a function of the amount and the nature of the ions added to the C12 matrix (b).

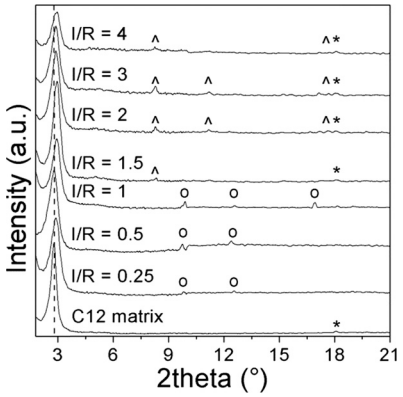

Fig. 3 Diffractograms of hybrid materials containing Ni and Mo ions. Nitric acid was systematically added to the copolymer solutions before raising the pH to 6.3–6.5 and the addition of the Ni and Mo ions. $(NH_4)_4[NiMo_6O_{18}(OH)_6]\cdot 5H_2O$ (^), NH_4NO_3 (*) and $(NH_4)_6Mo_7O_{24}\cdot 4H_2O$ (°) were identified.

composed of one Ni^{2+} ion coordinated by six MoO_6 octahedral units.[29,30]

No homogeneous hybrid can be obtained by mixing only Mo ions to the C12 matrix. $(NH_4)_6Mo_7O_{24}\cdot 4H_2O$ is indeed systematically detected and likely gathers the ion fraction that cannot interact with the C12 matrix (Fig. S1†). The addition of Mo ions also induces a slight increase (1.2 Å) of the C12 matrix d_{Bragg} (Fig. 2a, black squares).

The normalized area of the low-angle peak of several hybrid materials was also evaluated (Fig. 2b). It fluctuates but does not decrease significantly when Ni or both Ni and Mo ions are mixed to the C12 matrix. It even increases for hybrids having an I/R ratio = 1–2. The copolymer organization is thus not troubled within such hybrids. In contrast, this area progressively decreases when only Mo ions are added to the C12 matrix. This suggests that Mo ions rather disorganize the matrix instead of being regularly inserted inside it.

The MoO_4^{2-} anions are expected to establish electrostatic interactions with the copolymer positive ammonium groups. Such interactions stay difficult to be evidenced by spectroscopy. However, they can also be highlighted through a competition test involving two anions.[31] This is why diluted nitric acid was previously added to some copolymer solutions before raising the pH till 6.3 and the addition of Ni and Mo ions (see series of data noted by red diamonds for NiMo-C12 (HNO_3) on Fig. 2a). We observed that the presence of NO_3^- ions induces the crystallization of $(NH_4)_6Mo_7O_{24}\cdot 4H_2O$ within hybrids having an I/R ratio ≤ 1 (Fig. 3). Yet, heptamolybdate species are never detected within the hybrids prepared without nitric acid. This shows that the competition between NO_3^- and MoO_4^{2-} species troubles the MoO_4^{2-}–copolymer interactions. Consequently, the MoO_4^{2-} fraction that cannot be stabilized inside the matrix crystallizes independently of the matrix. In parallel, the nickel ions are believed to be inserted inside the matrix organization. When ion amounts larger than the I/R ratio = 1 are added to the matrix, $(NH_4)_4[NiMo_6O_{18}(OH)_6]\cdot 5H_2O$ and NH_4NO_3 are again detected on the diffractogram of the hybrids.

The addition of HNO_3 also increases the C12 matrix d_{Bragg} from 27.8 to 32.1 Å (Fig. 2a, see red diamond at I/R = 0). This effect reveals the insertion of nitrate ions (NO_3^-) inside the organized matrix. Then, the d_{Bragg} progressively decreases and is finally confined around 30.8 Å when the Ni and Mo ions are mixed with the C12 matrix. For the hybrid materials having an I/R ratio > 0.5, no more d_{Bragg} difference is observed independently of the presence of nitrate ions (Fig. 2a, red diamonds) or absence of nitrate ions (Fig. 2a, grey dots).

The hydration of the C12 matrix, of the ions alone and their corresponding hybrids was measured by TGA at 150 °C. The ion addition increases the water fraction trapped inside the C12 matrix. It also progressively dilutes the matrix within the hybrid materials. The use of diluting factors enables to deduce the water fraction of hybrids that originates from the natural copolymer hydration. Consequently, the water fraction increase linked to the addition of ions can be calculated (Table S1†). It corresponds to the difference between the measured water fraction and the original C12 matrix hydration. This reasoning reveals that mixing little ion amounts with the matrix (I/R ratio = 0.25) induces a pronounced increase of the water content of the hybrids. Then, from an I/R ratio > 0.5–1, the hydration evolves linearly with the ion quantity added to the copolymers (Fig. 4).

FTIR experiments were carried out to study the Ni–COO^- interactions (Fig. 5). The $\delta(CH_2)$ scissoring band, the antisymmetric stretching band of the COO^- moieties ($\nu_{as}^{COO^-}$) and the

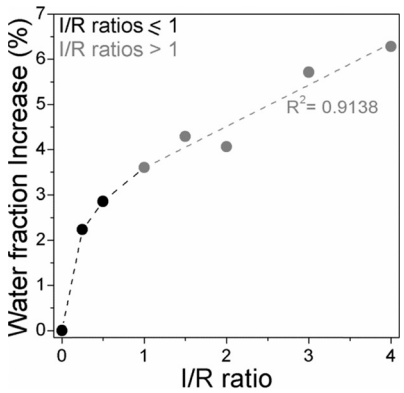

Fig. 4 Evolution of the increase of the water fraction trapped inside the hybrids as a function of the amount of Ni and Mo ions added to the C12 matrix.

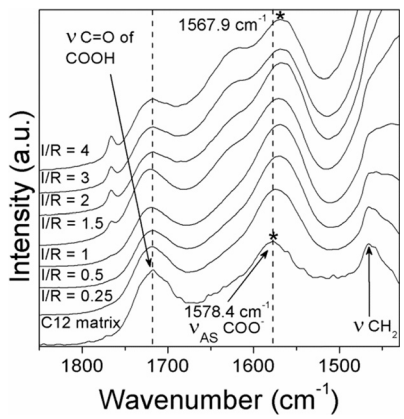

Fig. 5 FTIR spectra presenting the evolution of the position of the $\nu_{as}^{COO^-}$ band as a function of the amount of Ni and Mo ions added to the C12 matrix.

$\nu^{C=O}$ band (1726 cm^{-1}) linked to the COOH functions are systematically observed at 1466, 1578 and 1726 cm^{-1}, respectively.[32] The symmetric stretching band of the COO^- moieties ($\nu_{as}^{COO^-}$) is not visible here. Indeed, it is hidden by the broad and intense band at 1385 cm^{-1} attributed to the NO_3^- ions coming from $Ni(NO_3)_2{\cdot}6H_2O$.[33] The addition of Ni and Mo ions to the C12 matrix progressively shifts the $\nu_{as}^{COO^-}$ band from 1578 cm^{-1} to 1568 cm^{-1}. This band displacement reveals the coordination of the nickel ions by the COO^- functions. Its extent is proportional to the number of COO^- which interacts with the nickel ions.[24] The position of this band then remains stable from an I/R ratio = 1 even if larger ion amounts (I/R ratios > 1) are added to the matrix.

XPS experiments were carried out on hybrids containing nickel ions only. During the analyses, a partial decomposition of the C12 matrix and the nitrate ions is suspected due to the combined effects of X-rays and ultra-high vacuum. This is why the spectra acquisition time was optimized to obtain enough signal resolution as quickly as possible. Moreover, the analysis of the hybrid having an I/R ratio = 2 was repeated to evaluate the measurement variability.

The envelope of the Ni 2p doublet is complex because of the existence of satellite structures (Fig. 6). According to Grosvenor *et al.*, the position and the shape of the main Ni 2p peak (Ni $2p_{3/2}$) are affected by the electronegativity and the nature of the ligands linked to nickel.[34] The Ni $2p_{3/2}$ peak of nickel nitrate is observed at a binding energy (BE) of 856.5 eV.[9] This compound was used as a reference (Ni-inorganic contribution) where each nickel atom is coordinated by 6 water molecules. Hybrid materials having low Ni loadings (I/R ratio = 0.25–0.5) display this peak at lower BE (855.4–855.7 eV) which reflects the coordination of nickel by the copolymer COO^- functions.

A model was established in order to differentiate the nickel contribution stabilized inside the matrix (Ni-matrix) from the "Ni-inorganic contribution". The envelope of the Ni-matrix contribution was computed by combining the Ni $2p_{3/2}$ peak of the hybrids. The envelope of the Ni-matrix contribution was computed by combining the Ni $2p_{3/2}$ peak of the hybrids having low Ni loadings (I/R = 0.25–0.5).

This strategy supposed that the majority of the nickel present in these materials is indeed linked to the matrix. The calculated "Ni-matrix contribution" was then injected in the Ni $2p_{3/2}$ envelope of hybrid materials containing a larger Ni amount (I/R ratios > 0.5). The position of the injected Ni-matrix contribution was fixed between 855.4 and 855.7 eV as found for the materials having lower Ni loadings. Moreover, the width of this contribution was kept constant. A "Ni-inorganic contribution" was finally defined on the basis of the surface that remained uncovered by the Ni-matrix contribution. Interestingly, its shape and position on the BE axis looked like those of the Ni $2p_{3/2}$ peak of the nickel nitrate reference. Owing to the fact that both the Ni-matrix and Ni-inorganic contributions appear above 854 eV, one can state that the corresponding state of nickel cannot be

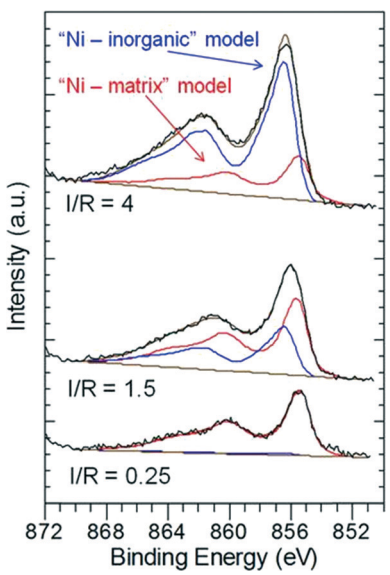

Fig. 6 Decomposition of the envelope of the Ni $2p_{3/2}$ XPS peak into a combination of two contributions namely the "Ni-matrix" contribution and the "Ni-inorganic" contribution.

metallic. Due to the complex structure of the Ni 2p contribution, it is difficult to further discriminate the oxidation state of Ni as either +2 or +3. However, as Ni is introduced as a Ni^{2+} nitrate salt in the hybrid, and as the hybridization does not involve any oxidation step, it sounds most likely that Ni remains in the hybrids in the +2 state. Besides, all the recorded spectra were decomposed as a sum of the two Ni-matrix and Ni-inorganic contributions (Fig. 6). For I/R ratios < 1, most of the nickel ions interact with the C12 matrix as no or only a little Ni-inorganic contribution is detected (Fig. 7). The nickel contribution linked to the matrix reaches a plateau around I/R ratios = 1–1.5 which reveals the C12 matrix saturation in nickel. In parallel, the contribution of inorganic nickel appears from an I/R ratio = 1 and dominates from an I/R ratio = 3.

The chemical environment of the nickel ions inside the C12 matrix was also characterized by ToF-SIMS. Two couples of peaks can be distinguished on the spectra of the hybrid materials, presented in Fig. 8: the couple m/z = 175.85, m/z = 177.85 and the couple m/z = 175.97, m/z = 177.97. They are related to anionic fragments containing at least one Ni atom as the gap between the peaks of each couple is equal to 2 m/z. Such a gap is indeed typical of the mass difference between a nickel atom (m/z = 58, abundance ≈ 68.1%) and its most abundant natural isotope (m/z = 60, abundance ≈ 26.2%).[35] It must be noted that ToF-SIMS experiments are managed under high vacuum which induces the removal of the nickel hydration sphere. The doublet m/z = 175.85 and m/z = 177.85 can then be assigned to the $[Ni_2CO_3]^-$ anion. The second peak doublet (m/z = 175.97 and m/z = 177.97) is attributed to the $[NiC_4O_4H_6]^-$ anion and was successfully identified by using a reference component: nickel(II) acetate tetrahydrate (>98%, Alfa Aesar). In fact, this anion corresponds to a dehydrated nickel atom coordinated by two acetate groups. It is responsible for the two main contributions on the spectrum of the reference component. Interestingly, this peak couple is also visible on the spectrum of the hybrid having an I/R ratio = 0.5. Corresponding shoulders can still be observed on the spectrum of the hybrid having an I/R ratio = 1. These results suggest that some nickel ions are coordinated by two COO^- moieties inside the C12 matrix.

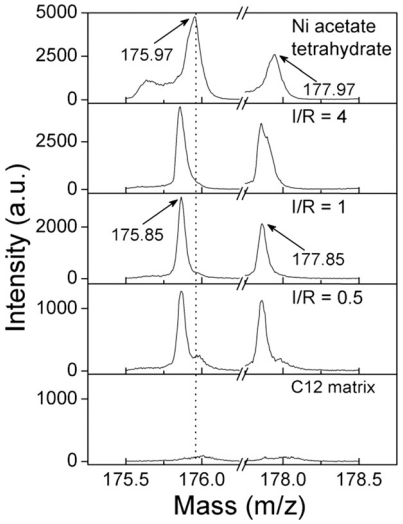

Fig. 8 Two narrow windows of the negative ToF-SIMS spectrum of nickel diacetate tetrahydrate (used as a reference), the C12 matrix and hybrid materials containing Ni ions only.

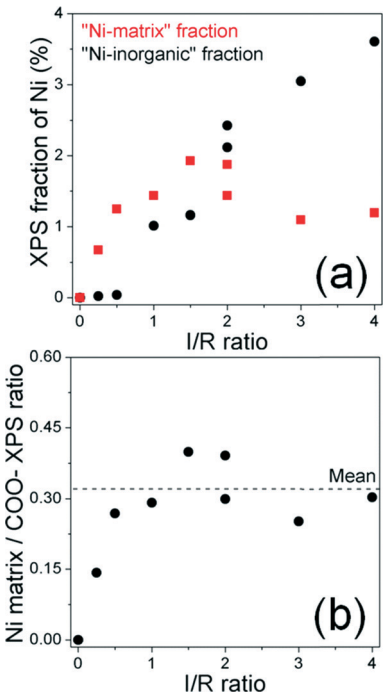

Fig. 7 Evolution of the "Ni-matrix" (red squares) and "Ni-inorganic" (black dots) contributions as a function of the nickel amount added to the C12 matrix (a). Evolution of the "Ni matrix"/COO^- molar ratio as a function of the nickel amount added to the C12 matrix (b). The COO^- functions were quantified from the contribution at BE ~ 288.5 eV of the C 1s XPS peak.

Properties and catalytic behaviour of $NiMoO_4$

In agreement with the literature, the co-precipitated oxide (NiMo-Cop) displays α-$NiMoO_4$ as the main crystalline phase.[23,36] One minor signal also reveals the presence of a few β-crystals in NiMo-Cop (Fig. 9). The calcination at 475 °C of a hybrid having an I/R ratio = 4 leads to the coexistence of both α and β phases with α-$NiMoO_4$ being dominant. In contrast, a major β-phase is obtained after the calcination of hybrids having an I/R ratio = 1. Fig. S2† shows the progressive decrease of the β to α content ratio in the calcined materials as a function of the I/R ratio in the hybrids.

According to the IUPAC nomenclature, the NiMo-Cop sample displays a type II isotherm which indicates its non-porous nature (Fig. 10).[37,38] This solid is likely finely divided as it possesses a not so small specific surface area (38.4 $m^2\ g^{-1}$). Calcined hybrids present similar specific surface areas but exhibit type IV isotherms (Fig. 10). Additionally, their adsorption and desorption isotherms reveal at high relative pressures (0.46–0.98) a hysteresis loop being a mix between the H_3- and the H_2-types.[37,38] These features are typical of

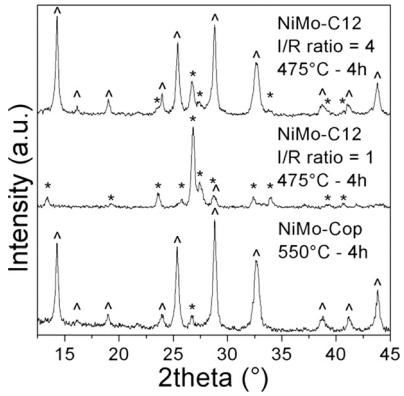

Fig. 9 Diffractograms of materials made *via* co-precipitation and from hybrid precursors. β-$NiMoO_4$ (*) and α-$NiMoO_4$ (^) were identified.

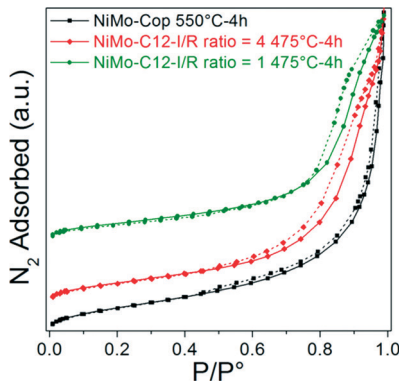

Fig. 10 Adsorption (solid line) and desorption (dashed line) N_2 physisorption isotherms of materials made *via* co-precipitation and from hybrid precursors.

mesoporous materials having mesopores that result from the liberation of volume due to the degradation of carbon matter.[37,39] The total pore volume of 0.13 cm g^{-1} was evaluated for the solid obtained by calcination of the hybrid NiMo-C12 I/R = 1. Next to a small population of mesopores of about 2 to 4 nm in diameter, the main fraction of this volume is brought by mesopores having a diameter of 9 nm.

SEM confirmed the finely divided nature of the coprecipitated $NiMoO_4$ which consists of the aggregation of nanometric hair-like particles entangled together and forming cauliflower bunches of undefined shapes (Fig. 11; left). The material obtained by calcination of the NiMo-C12 I/R = 1 hybrid consists of granular particles smaller than 100 nm, assembled together in platelets giving them a layered morphology at the micrometric level (Fig. 11, right).

XPS results available in the ESI† (Table S2) show that the oxidation states of the Ni and Mo atoms in our $NiMoO_4$ are 2+ and 6+, respectively. Such a result is consistent with the facts that the hybrids (i) were made from salts where the metals were present at the 2+ and 6+ states, too, and (ii) were converted to the catalysts for 4 h under air.

After an equilibration period of about one hour, the performance of the catalysts was stable along the three additional hours during which the test was performed. As a representative example, Fig. S3† presents the evolution with time-on-stream of the propane conversion on NiMo-C12 I/R = 1 obtained by calcination of the hybrid at 475 °C. Table 1 compiles the performance of the catalysts averaged on the whole test. The oxides characterized above present a similar propane conversion in the range of 10%. Such a quasi-isoconversion situation was required to directly compare the selectivities of the different catalysts. Actually, the necessity to work as close as possible to isoconversion explained why the NiMo-Cop catalyst was obtained by calcination of the coprecipitated precursor at a higher temperature (550 °C) than the hybrid ones (475 °C). Such a high calcination temperature enables to reach a surface area close to that of the NiMo-C12 samples (in the range of 35 m^2 g^{-1}). A similar conversion level could thereby be reached using 150 mg of catalyst whatever the catalyst. Thus comparing the selectivities of the different catalysts, NiMo-Cop deeply oxidizes propane into CO_x as its CO (20.1%) and CO_2 (64.6%) selectivities are both superior to its propene selectivity (14.4%) (Table 1). Calcined hybrids produce propene more selectively (72% the catalyst prepared from the I/R = 1 hybrid and 56.3% for the one prepared from the I/R = 4) to the detriment of CO_2 and CO. Traces of ethene, acrolein, acetone, propanal and acetaldehyde were also detected but the sum of their selectivities never exceeds 5% (not shown). Thanks to their high propene selectivity, the calcined hybrids display a superior propene yield to NiMo-Cop. It could be argued that the comparison of the selectivities was not done at perfect isoconversion, and that this comparison is thus not relevant. However, as usually the selectivity to CO_x increases when the conversion at which the catalyst is operated is higher, and as our most selective catalyst, namely NiMo-C12 I/R = 1, exhibited a slightly higher conversion than the others, this reinforces the conclusion that the catalysts prepared from the hybrid precursors are indeed really more selective to propene than the reference $NiMoO_4$ material prepared *via* the classical coprecipitation route.

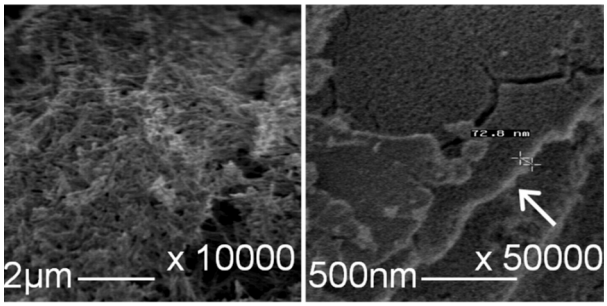

Fig. 11 SEM pictures of $NiMoO_4$ obtained by calcination of the coprecipitated precursor (left) and the NiMo-C12 I/R = 1 hybrid (right).

Discussion

Establishment of a model

The self-assembled C12 matrix presents a supramolecular organization thanks to the hydrophobic interactions between

Table 1 Specific surface area (Ss), propane conversion ($C_{propane}$), product selectivities ($S_{product}$) and propene yield ($Y_{propene}$) of catalysts made *via* co-precipitation and from hybrid precursors. The catalytic performance was measured at 475 °C

Catalyst	Ss ($m^2\ g^{-1}$)	$C_{propane}$ (%)	$S_{propene}$ (%)	S_{CO_2} (%)	S_{CO} (%)	$Y_{propene}$ (%)
NiMo-Cop	38.4	12.0	14.4	64.6	20.1	1.7
NiMo-C12 I/R = 1	33.3	14.1	72.0	17.9	4.7	10.2
NiMo-C12 I/R = 4	37.5	8.7	56.3	40.6	2.3	4.9

its dodecyl side chains. For such a comb-like copolymer, Rullens *et al.* envisaged a lamellar model based on the alternation of crystallized hydrophobic microdomains and amorphous hydrophilic microdomains (Scheme 1).[15,16] The FTIR results reveal the coordination of the nickel ions by the copolymer COO^- functions whereas XRD highlight an increase of the C12 matrix d_{Bragg} when the nickel ions are added to it (Fig. 2 and 5). By correlating these results, the Ni–COO^- interactions appear responsible for the expansion of the matrix organization due to the insertion of the nickel ions (Fig. 12).[28] These ions are likely inserted inside the copolymer hydrophilic region because of their polar nature. Besides, the oversized nature of the MoO_4^{2-} anions (ionic diameter: 5.4 Å) makes their insertion between the copolymer backbones not plausible.[40] In fact, these ions are rather expected to establish electrostatic interactions with the positive ammonium groups in the inter-sheet space located in between two copolymer layers (Scheme 2).

The increase of the C12 matrix d_{Bragg} and the shift of the $\nu_{as}^{COO^-}$ band are both maximized and stabilized at the I/R ratio = 1 (Fig. 12). This indicates the matrix saturation in the nickel ions when the I/R ratio = 1 is reached. One nickel ion and one molybdenum ion can then at best be hybridized per two copolymer repeating units. An additional larger ion amount (I/R ratio > 1) cannot be inserted inside the C12 matrix anymore and induces the crystallization of $(NH_4)_4[NiMo_6O_{18}(OH)_6]\cdot 5H_2O$ (Fig. 1). These materials are considered to be heterogeneous whereas those having an I/R ratio ≤ 1 are homogeneous.

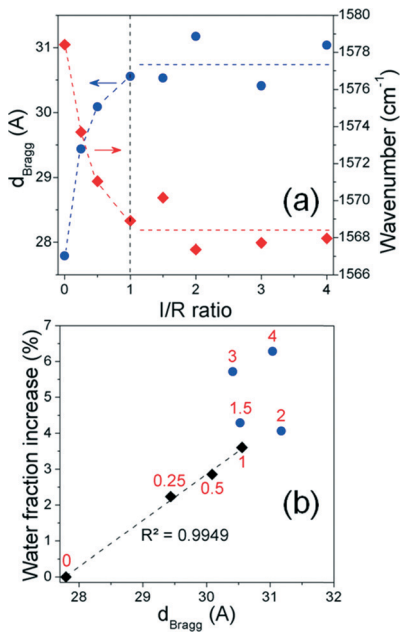

Fig. 12 Evolution of the copolymer d_{Bragg} (blue circles) and the $\nu_{as}^{COO^-}$ band position (red diamonds) as a function of the amount of Ni and Mo ions added to the C12 matrix (a). Correlation between the copolymer d_{Bragg} and the increase of the water fraction trapped inside the hybrids (I/R ratio ≤ 1: black diamonds, and I/R ratio > 1: blue circles) (b).

The C12 matrix contains 4.9 wt% of water (Table S1†). This represents 1.1 water molecules per copolymer repeating unit. This structural water is probably trapped inside the hydrophilic regions of the matrix organization. The addition of ions raises the water fraction measured within the hybrid materials (Fig. 4). The correlation between the XRD and TGA results reveals that this water fraction increases proportionally with the matrix d_{Bragg} until reaching an I/R ratio = 1 (Fig. 12). The C12 matrix expansion promoted by the nickel insertion thus induces an additional water encapsulation inside the copolymer hydrophilic regions (1.4 supplementary water molecules per repeating unit for an I/R ratio = 1). Beyond the saturation, the further addition of ions (I/R ratios > 1) induces a less marked increase of the hybrid hydration and no further d_{Bragg} variation is noticed anymore (Fig. 12). This tendency is related to the crystallization out of the C12 matrix of $(NH_4)_4[NiMo_6O_{18}(OH)_6]\cdot 5H_2O$ and NH_4NO_3 and to their natural predisposition to be hydrated: 9.6 wt% of water (Table S1†). In fact, the hydration of the saturated hybrids (I/R ratio > 1) proportionally increases with the ion excess that is not inserted within the C12 matrix (Fig. 4).

More about the Ni–COO^- interactions

As stated before, the nickel ions are coordinated by the copolymer COO^- functions within the hybrids (Fig. 5). However, several coordination modes are distinguished in the literature (Scheme S1).[24] The bridging and chelating bonds usually shift the $\nu_{as}^{COO^-}$ band to higher wavenumbers. Furthermore, splitting of this band is often observed. These coordination modes can be discarded as the addition of nickel here shifts the $\nu_{as}^{COO^-}$ band to lower wavenumbers. Such a weak band downward shift (10 cm^{-1}) is rather consistent with monodentate Ni–COO^- complexes. It reflects the formation of weak complexes which do not strongly affect the force constant of the two C=O bonds of a carboxylate moiety. The equivalence between these bonds is thus preserved. The monodentate coordination mode can be seen as a flexible bond where the nickel is not kept at a fixed position with respect to the COO^- moiety.[24] However, a small $\nu_{as}^{COO^-}$ band shift may also suggest that only a fraction of the copolymer COO^- functions

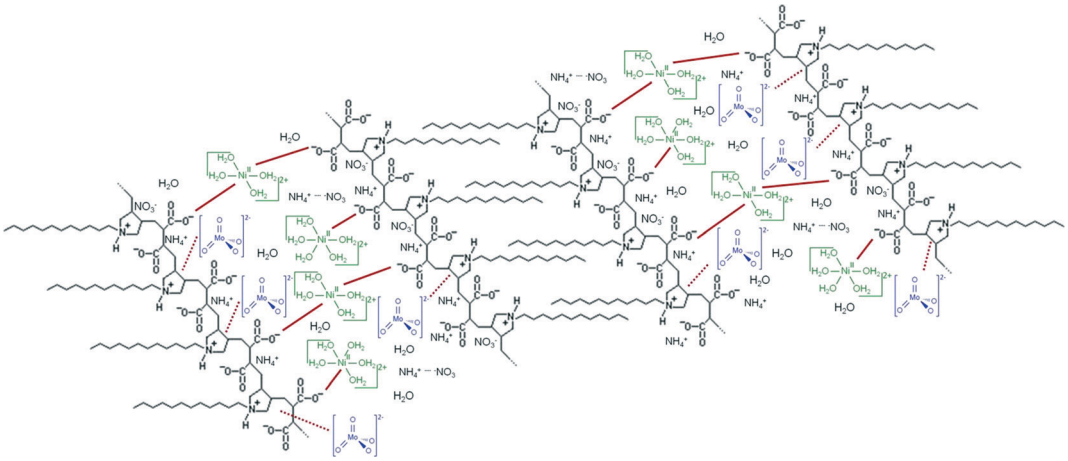

Scheme 2 Model designed for a homogeneous hybrid (I/R ratio = 1). MoO_4^{2-}–NHR_3^+ bonds go out of the matrix organization plane (dotted lines).

really interacts with the nickel ions.[24] At the matrix saturation (I/R ratio = 1), the Ni/COO^- ratio equals 0.25 (0.5 mol of Ni ions per 1 mol of copolymer repeating unit) which confirms the idea that all the COO^- are not coordinated to a nickel ion. In fact, both hypotheses appear plausible here. It can therefore be concluded that the C12 matrix saturation is reached when only a fraction of the COO^- is coordinated to nickel through weak monodentate coordination bonds.

A model approach based on the XPS results enables us to distinguish and quantify the 2 different nickel states within the hybrid materials containing only nickel ions: the inorganic nickel and the nickel linked to the C12 matrix (Fig. 6). The latter reaches a plateau around an I/R ratio = 1–1.5 which reflects the matrix saturation in nickel already evoked by the XRD results (Fig. 2). This quantification also reveals the coexistence of both nickel states inside hybrids having an I/R ratio $>$ 0.5. This suggests that all the nickel ions of hybrids having an I/R ratio = 1 are not necessarily coordinated by the COO^- moieties. However, the Ni-matrix contribution is likely underestimated due to the combined effects of X-rays and ultra-high vacuum. Indeed, the degradation of the COO^- moieties linked to nickel should artificially increase the Ni-inorganic fraction. Normalizing the Ni-matrix fraction with the detected (and thus not degraded) amount of COO^- functions helps to get rid of that unwanted side effect. A Ni-matrix/COO^- molar ratio of 0.29 is calculated at the C12 matrix saturation (I/R ratio = 1, Fig. 7). This estimation is consistent with the one calculated from the XRD–FTIR results: Ni/COO^- = 0.25 (Fig. 10). Thereby, we conclude that the majority of the nickel ions of the hybrid materials having an I/R ratio = 1 does effectively interact with the COO^- functions of the matrix.

At excessive nickel amounts (I/R ratio $>$ 1), the nickel precipitation and its crystallization into $Ni_2(NO_3)_2(OH)_2{\cdot}2H_2O$ cannot be avoided because of the relatively low solubility of nickel in aqueous solution from pH 6 (Fig. 1). In fact, the formation of a precipitate pumps the nickel ions out of the matrix and thus partially prevents their insertion inside the copolymers. This is why hybrids having an I/R ratio $>$ 1 and containing nickel ions only present a lower d_{Bragg} with respect to those having an I/R ratio = 1 (Fig. 2). At the matrix saturation (I/R ratio = 1), the copolymer expansion is maximal (d_{Bragg} = 30.7 Å) as most of the nickel ions can interact with the matrix without constraint (Fig. 2). However, the weakness and the reversibility of the Ni–COO^- coordination bonds should always be kept in mind. The complexation of Ni by the COO^- functions is then never completely achieved. But, this does not mean that the engaged ions are not well-dispersed inside the hydrophilic regions of the homogeneous hybrids (I/R ratio $\leq$ 1). In fact, an equilibrium between the coordination mode and an electrostatic mode can be imagined where both contribute to disperse the Ni ions along the copolymers. The matrix expansion due to the Ni insertion and the absence of $Ni_2(NO_3)_2(OH)_2{\cdot}2H_2O$ crystals argue in favor of this hypothesis for these hybrids (Fig. 2).

Nickel as a stabilizer of the C12 matrix organization

The addition of Mo ions instead of Ni ions induces a smaller expansion of the C12 matrix organization (Fig. 2). However, its main effect is the matrix disorganization. This phenomenon is linked to the electrostatic bonds that the copolymers establish with the MoO_4^{2-} anions. (Fig. 1 and 2). These interactions are believed to be stronger than the hydrophobic interactions behind the matrix organization. As a result, the electrostatic interactions promote a copolymer reorganisation around the MoO_4^{2-} anions. In contrast, the original copolymer organization is not affected by the addition of the nickel ions. Actually, it is improved within hybrids having an I/R ratio = 1–2 (Fig. 2). This tendency remains valid in the presence of both Ni and Mo ions. Thereby, it is understood that the Ni ions preserve the C12 matrix from the disorganization effects induced by the MoO_4^{2-} anions. Several authors demonstrated that the coordination of a Ni ion by a COO^- group is not discordant with the capacity of this ion to link simultaneously several COO^- functions.[24,41,42] Consequently, two copolymers delimiting a hydrophilic microdomain could be

bridged through the formation of a complex involving one nickel ion and one COO^- group of each macromolecule (Scheme 2). Such bonds would contribute to stabilize and even strengthen the C12 matrix organization. XRD and ToF-SIMS experiments provided some clues in favor of this hypothesis.

Compared to the nickel ions, the insertion of NO_3^- induces a larger expansion of the copolymer organization (d_{Bragg} = 32.1 Å *vs.* 30.7 Å) (Fig. 2). However, the subsequent addition of Ni and Mo ions contracts the copolymer d_{Bragg} and finally confines it around 30.8 Å. For hybrids having an I/R ratio > 0.5, no more d_{Bragg} difference is observed independently of the presence or absence of NO_3^-. The nickel ions are thus able to constrain the C12 matrix d_{Bragg} in a fixed interval regardless of the initial value. The establishment of $RCOO^-$–Ni–$RCOO^-$ complexes could be a reliable hypothesis to explain this observation. The results of the ToF-SIMS experiments are in agreement with this hypothesis. Signals attributed to the $[NiC_4O_4H_6]^-$ anion are visible on the SIMS spectrum of hybrids having an I/R ratio = 0.5 and 1 and containing Ni ions only (Fig. 8). Their presence confirms the capacity of the nickel ions to be linked to two COO^- moieties. The concentration of the $[NiC_4O_4H_6]^-$ fragment should be maximized at the copolymer saturation in nickel (I/R ratio = 1). The addition of an excessive nickel amount (I/R ratio = 4) complicates the detection of these fragments due to a dilution effect. Experimental limitations inherent to the ToF-SIMS technique prevent quantitative estimations. Moreover, the $[NiC_4O_4H_6]^-$ ion also possesses a weak ionization probability because of the numerous chemical bonds that need to be broken to extract it from the hybrid structure. Consequently, the small signals assigned to the $[NiC_4O_4H_6]^-$ fragment do not necessarily reflect its concentration within the hybrids. In the end, this complex can be quite concentrated and strongly contributes to stabilize the C12 matrix organization.

Toward better efficiency of $NiMoO_4$ in the ODHP reaction

The calcination of the hybrids induces the crystallization of β-$NiMoO_4$. This phase is normally metastable at RT, and makes NiMo-based materials far more selective to propene in the ODHP reaction.[9] The exothermic degradation of carbon matter seems to be the key point. This degradation induces a rapid crystallization that cannot involve all the nickel ions available within the precursor.

The remaining nickel fraction is then expected to be dispersed across the β-$NiMoO_4$ network and prevents the β → α-$NiMoO_4$ relaxation.[9,43] Furthermore, defects linked to a rapid and imperfect crystallization may contribute to stabilizing this β-phase. The exothermic combustion of the matrix also supplies the heat for the β-$NiMoO_4$ crystallization at moderate temperatures (475 °C) whereas strong temperatures (>650 °C) are usually required. The pore volume liberated by the matrix degradation can then be preserved from sintering.[18] It is likely that the micrometric layered morphology of the $NiMoO_4$ material obtained from the homogenous NiMo-C12 I/R = 1 hybrid (Fig. 11) is reminiscent of the supramolecular organization of the C12 matrix which was maintained after the incorporation of the Ni and Mo ions (Scheme 2). In the end, $NiMoO_4$ having an acceptable specific surface area is prepared which maintains its activity level quite high as well. Compared to the NiMo-Cop sample under the same reaction conditions, a higher propene selectivity coupled with a similar propane conversion makes the calcined hybrids six times more efficient to produce propene. Note that the NiMo-Cop catalyst was obtained by calcination at a higher temperature than the hybrid precursors (the reason why is explained in the last paragraph of the Results section), which could be criticized. One has to realize that subjecting the coprecipitated precursor to a lower calcination temperature would have led to an even higher fraction of α-$NiMoO_4$ in the final catalyst. This would have finally led to a worse propene selectivity, which reinforces the superiority of the catalysts prepared from the hybrids. However, the use of heterogeneous hybrids (I/R ratio = 4) is not recommended. In fact, their ion excess cannot benefit from the heat released by the combustion of carbon matter being not in its close environment. This leads to a substantial α-$NiMoO_4$ crystallization and makes the calcined hybrids less selective to propene. This statement is in agreement with the preliminary results.[22] It also underlines the necessity to effectively disperse all ions inside the matrix thanks to the interactions with the copolymer's charged moieties.

Conclusions

Homogeneous hybrid materials (I/R ratio ≤ 1) associating Ni and Mo ions and a self-assembled copolymer were successfully synthesized at pH 6.3–6.5. In such a condition, each copolymer repeating unit possesses one positive charge and two negative charges. Thereby, the number of copolymer charges and its capacity to fix ions are both maximized. The addition of excessive ion amounts (I/R ratio > 1) induces the crystallization of $(NH_4)_4[NiMo_6O_{18}(OH)_6]\cdot 5H_2O$ independently of the matrix which makes the hybrids heterogeneous. Electrostatic interactions enable to disperse the MoO_4^{2-} anions within the hybrids but also disorganize the C12 matrix. The coordination of the nickel ions with the copolymer COO^- functions prevents this effect. By bridging two macromolecules, the nickel ions indeed reinforce the C12 matrix organization and allow the preparation of organized and nanostructured hybrid materials.

Our use of supramolecularly organized precursors and the possibility it offers to form $NiMoO_4$ under "soft conditions" lead to mesoporous β-$NiMoO_4$ stable at RT. The phase was targeted as it is the most selective to propene in the ODHP reaction. However, β-$NiMoO_4$ is usually metastable in contrast to α-$NiMoO_4$ which is stable at RT. Its preparation generally also requires high temperatures which favours sintering and makes it poorly active in the ODHP reaction. Here, we have succeeded in generating the most propene selective β-phase without sacrificing its specific surface area,

and thus maintaining its activity remarkably high as well. The use of heterogeneous hybrids should be avoided as it promotes substantial α-$NiMoO_4$ crystallisation that is detrimental for the propene selectivity and the propene yield of NiMo-based materials.

Abbreviations

XRD	X-ray diffraction
XPS	X-ray photoelectron spectroscopy
FTIR	Fourier transform infrared spectroscopy
TGA	Thermogravimetric analysis
ToF-SIMS	Time-of-flight-secondary ion mass spectroscopy
ODHP	Oxidative dehydrogenation of propane
Ni	Nickel ion
Mo	Molybdenum ion
I/R ratio	Inorganic ion per copolymer repeating unit molar ratio

Acknowledgements

The authors thank R. Lasselin for the copolymer preparation. The authors also gratefully acknowledge the '*Fonds pour la formation à la Recherche dans l'Industrie et dans l'Agriculture* (*FRIA*)' of Belgium for financial support and B. Farin's PhD fellowship. Finally, the institute is indebted to the '*communauté française de Belgique*' for financial support through the ARC programme (08/13-009).

Notes and references

1 D. P. Debecker, V. Hulea and P. H. Mutin, *Appl. Catal., A*, 2013, **451**, 192–206.
2 S.-H. Chai, H.-P. Wang, Y. Liang and B.-Q. Xu, *Appl. Catal., A*, 2009, **353**, 213–222.
3 M. C. Kroon, D. Hartmann and A. J. Berkhout, *Ind. Eng. Chem. Res.*, 2008, **47**, 8517–8525.
4 M. M. Bettahar, G. Costentin, L. Savary and J. C. Lavalley, *Appl. Catal., A*, 1996, **145**, 1–48.
5 F. Cavani, N. Ballarini and A. Cericola, *Catal. Today*, 2007, **127**, 113–131.
6 K.-H. Kim and S.-K. Ihm, *J. Hazard. Mater.*, 2011, **186**, 16–34.
7 Q. H. Xia, H. Q. Ge, C. P. Ye, Z. M. Liu and K. X. Su, *Chem. Rev.*, 2005, **105**, 1603–1662.
8 H. Balcar and J. Čejka, *Coord. Chem. Rev.*, 2013, **257**, 3107–3124.
9 L. M. Madeira, M. F. Portela and C. Mazzocchia, *Catal. Rev.: Sci. Eng.*, 2004, **46**, 53–110.
10 D. L. Stern and R. K. Grasselli, *J. Catal.*, 1997, **167**, 550–559.
11 M. A. Botavina, G. Martra, Y. A. Agafonov, N. A. Gaidai, N. V. Nekrasov, D. V. Trushin, S. Coluccia and A. L. Lapidus, *Appl. Catal., A*, 2008, **347**, 126–132.
12 A. Maione and M. Devillers, *J. Solid State Chem.*, 2004, **177**, 2339–2349.
13 A. Kaddouri, E. Tempesti and C. Mazzocchia, *Mater. Res. Bull.*, 2004, **39**, 695–706.
14 C. Mazzocchia, R. Anouchinsky, A. Kaddouri, M. Sautel and G. Thomas, *J. Therm. Anal.*, 1993, **40**, 1253–1265.
15 K. Inomata, Y. Sakamaki, T. Nose and S. Sasaki, *Polym. J.*, 1996, **28**, 992–999.
16 F. Rullens, M. Devillers and A. Laschewsky, *Macromol. Chem. Phys.*, 2004, **205**, 1155–1166.
17 W.-H. Zhang, L. Zhang, J. Xiu, Z. Shen, Y. Li, P. Ying and C. Li, *Microporous Mesoporous Mater.*, 2006, **89**, 179–185.
18 D.-S. Wang, T. Xie, Q. Peng, S.-Y. Zhang, J. Chen and Y.-D. Li, *Chem. – Eur. J.*, 2008, **14**, 2507–2513.
19 P. Favresse and A. Laschewsky, *Polymer*, 2001, **42**, 2755–2766.
20 F. Rullens, M. Devillers and A. Laschewsky, *J. Mater. Chem.*, 2004, **14**, 3421–3426.
21 F. Rullens, N. Deligne, A. Laschewsky and M. Devillers, *J. Mater. Chem.*, 2005, **15**, 1668–1676.
22 B. Farin, C. Swalus, M. Devillers and E. M. Gaigneaux, *Catal. Today*, 2013, **203**, 24–31.
23 R. Del Rosso, A. Kaddouri, C. Mazzocchia, P. Gronchi and P. Cèntola, *Catal. Lett.*, 2000, **69**, 71–78.
24 T. J. Strathmann and S. C. B. Myneni, *Geochim. Cosmochim. Acta*, 2004, **68**, 3441–3458.
25 H. K. Hall, *J. Am. Chem. Soc.*, 1957, **79**, 5441–5444.
26 B. Beverskog and I. Puigdomenech, *Corros. Sci.*, 1997, **39**, 969–980.
27 L. E. Briand, G. M. Valle and H. J. Thomas, *J. Mater. Chem.*, 2002, **12**, 299–304.
28 M. Alexandre and P. Dubois, *Mater. Sci. Eng., R*, 2000, **28**, 1–63.
29 A. Sampieri, S. Pronier, S. Brunet, X. Carrier, C. Louis, J. Blanchard, K. Fajerwerg and M. Breysse, *Microporous Mesoporous Mater.*, 2010, **130**, 130–141.
30 L. C. W. Baker and D. C. Glick, *Chem. Rev.*, 1998, **98**, 3–50.
31 E. Guibal, *Sep. Purif. Technol.*, 2004, **38**, 43–74.
32 N. Kameta, M. Masuda, H. Minamikawa and T. Shimizu, *Langmuir*, 2007, **23**, 4634–4641.
33 T. N. Ramesh and P. V. Kamath, *J. Power Sources*, 2006, **156**, 655–661.
34 A. P. Grosvenor, M. C. Biesinger, R. S. C. Smart and N. S. McIntyre, *Surf. Sci.*, 2006, **600**, 1771–1779.
35 G. Audi, O. Bersillon, J. Blachot and A. H. Wapstra, *Nucl. Phys. A*, 2003, **729**, 3–128.
36 C. Mazzocchia, C. Aboumrad, C. Diagne, E. Tempesti, J. M. Herrmann and G. Thomas, *Catal. Lett.*, 1991, **10**, 181–191.
37 K. S. W. Sing, D. H. Everett, R. A. W. Haul, L. Moscou, R. A. Pierotti, J. Rouquerol and T. Siemieniewska, *Pure Appl. Chem.*, 1984, **57**, 567–583.
38 M. Kruk and M. Jaroniec, *Chem. Mater.*, 2001, **13**, 3169–3183.
39 S. S. Kim, W. Zhang and T. J. Pinnavaia, *Science*, 1998, **282**, 1302–1305.
40 K.-H. Goh, T.-T. Lim and Z. Dong, *Water Res.*, 2008, **42**, 1343–1368.
41 Y. Dan and Q. Wang, *Polym. Int.*, 2001, **50**, 1109–1114.
42 G. B. Deacon and R. J. Phillips, *Coord. Chem. Rev.*, 1980, **33**, 227–250.
43 R. Anouchinsky, A. Kaddouri and C. Mazzocchia, *J. Therm. Anal.*, 1996, **47**, 299–309.

